

# Ground-State Phase Diagram of the $S = 1$ One-Dimensional Kondo Lattice Model with a Uniaxial Anisotropy under Transverse Fields

Kohei Suzuki and Kazumasa Hattori

*Department of Physics, Tokyo Metropolitan University, 1-1 Minami-osawa, Hachioji, Tokyo 192-0397, Japan*

We study the effects of transverse magnetic fields on the  $S = 1$  one-dimensional Kondo lattice model with a uniaxial anisotropy using the density matrix renormalization group. The model can be regarded as a simplified one for analyzing the Ising ferromagnetic superconductor URhGe. We find various phases such as ferromagnetic and antiferromagnetic phases, Kondo plateau (KP) phases, Tomonaga-Luttinger liquids, and fully polarized phases. In the KP phase, a pseudo-plateau emerges in the magnetization due to strongly bound pairs between the local and the conduction electron spins. This is why we call this phase the Kondo plateau. At the critical field between the ferromagnetic and KP phases, we find metamagnetic behavior in the magnetization curve. We discuss various correlation functions and the Friedel oscillations in detail, and the experimental data under transverse magnetic fields in URhGe are discussed on the basis of the present results.

## 1. Introduction

The coexistence of ferromagnetism and superconductivity (SC) has attracted considerable attention since the discovery in  $\text{UGe}_2$ .<sup>1)</sup> Since then, some other materials showing both ferromagnetism and SC have been found, such as URhGe,<sup>2)</sup> UIr,<sup>3)</sup> and UCoGe.<sup>4)</sup> Among them, URhGe and UCoGe have been discussed in considerable detail in recent years.<sup>5–8)</sup> They show SC inside their ferromagnetic (FM) state in ambient pressure.<sup>2,4)</sup> One of the common properties of the U-based FM superconductors is their strong Ising anisotropy, and strongly anisotropic magnetic fluctuations have been observed in NMR experiments.<sup>9–12)</sup>

For URhGe, the Ising FM order takes place at  $T_c \sim 9.5$  K, and the moment size is about  $0.4\mu_B$  along the c-axis. The SC emerges inside the FM state at  $T_{sc} = 0.26$  K and disappears for the magnetic field  $H = 2$  T along the b-axis. However, another SC emerges when the field increases further ( $H \sim 9$  T).<sup>5)</sup> This is called reentrant SC (RSC). This RSC emerges near the critical magnetic field along the b-axis, above which the FM state disappears and the moment is polarized along the b-axis. Thus, the origin of the RSC is considered to be related to the physics of the transverse-field Ising model (fluctuation), a well-known model that possesses a quantum criticality.<sup>13)</sup> Detailed experimental investigations have revealed that the transition is first-order and there is a tricritical point at a finite temperature,<sup>14,15)</sup> while there is a smooth change in the thermodynamic quantities such as the magnetization.<sup>16)</sup> This suggests that it is a “weak” first-order transition. Indeed, the magnetization strongly increases inside the RSC phase, which is typical metamagnetic behavior. This is also reflected in the relaxation time  $T_2$  in the NMR experiment,<sup>9)</sup> in which  $1/T_2$  shows strong enhancement.

Regarding theoretical analyses, several works have been carried out,<sup>17–24)</sup> which include studies on SC mediated by spin-wave excitations near the critical field<sup>18)</sup> and by phe-

nomenological spin fluctuations,<sup>23)</sup> and SC near Lifshitz transitions.<sup>24)</sup> Inevitable line nodes in the superconducting gap functions characteristic of the nonsymmorphic zigzag chain structure along the a-axis have been pointed out recently,<sup>25)</sup> and also an interesting topological SC for UCoGe has been proposed.<sup>26)</sup>

In this paper, we focus on the effects of transverse magnetic fields in the Kondo lattice model with strong Ising anisotropy. To simplify the analysis, we consider the one-dimensional model and the local spin  $S = 1$ . The first simplification corresponds to ignoring inter-chain couplings in URhGe and related compounds. The second one, taking the  $S = 1$  model, enables us to discuss the uniaxial single-ion anisotropy while maintaining the essential property of the U-based FM SCs. This is the lowest spin that has the uniaxial anisotropy, and the analysis becomes much simpler than that for the larger spin.

For more than two decades, a number of studies about the  $S = 1/2$  Kondo lattice model have been carried out.<sup>27–32)</sup> In the one-dimensional Kondo lattice model, it is well known that the FM state appears for the strong Kondo coupling region.<sup>33–37)</sup> The existence of other FM phases has also been discussed recently.<sup>38–42)</sup> In contrast, for larger spin models, including the  $S = 1$  one, it has not been studied in detail so far. The  $S = 1$  Kondo lattice model has been analyzed on the basis of mean-field theory<sup>43,44)</sup> to discuss U-based heavy fermions. For impurity Kondo models, the Kondo model with an  $S = 1$  local spin interacting with  $s = 3/2$  conduction electrons has been discussed and shown to be an exotic non-Fermi liquid.<sup>45)</sup> Although much attention has been paid to the SC under magnetic fields in URhGe and UCoGe, there is no study focusing on the ground-state properties and the phase diagram for microscopic models with strong Ising anisotropy in the Kondo lattice systems. Thus, it is important to analyze the  $S = 1$  Kondo lattice model and to construct the phase diagram under transverse fields. To carry out the quantitative

analysis, we employ the density matrix renormalization group (DMRG),<sup>46)</sup> which is a well-known powerful numerical tool for analyzing one-dimensional systems.

This paper is organized as follows. In Sect. 2, the model used in this study and some of the details of the DMRG specific to the model are introduced. Then, we will show the numerical results, which include ground-state phase diagrams and various correlation functions in Sect. 3. In Sect. 4, we will discuss our numerical results by comparing them with experimental data in URhGe, and finally, we will summarize the present results.

## 2. Model

In this section, we will introduce the model and explain its basic properties. The Hamiltonian of the  $S = 1$  one-dimensional Kondo lattice model with a uniaxial anisotropy  $D$  under a transverse field  $h$  is given as

$$\hat{H} = -t \sum_{j=1}^{N-1} \sum_{\sigma=\uparrow,\downarrow} \left( \hat{c}_{j\sigma}^\dagger \hat{c}_{j+1\sigma} + \hat{c}_{j+1\sigma}^\dagger \hat{c}_{j\sigma} \right) + J \sum_{j=1}^N \hat{s}_j \cdot \hat{S}_j - h \sum_{j=1}^N \left( \hat{s}_j^x + \hat{S}_j^x \right) - D \sum_{j=1}^N \left( \hat{s}_j^z \right)^2. \quad (1)$$

Here,  $N$  is the system size and  $\hat{c}_{j\sigma}$  is the annihilation operator of the conduction electron at the  $j$  site with the spin  $\sigma = \uparrow$  or  $\downarrow$ .  $\hat{s}_j = (\hat{s}_j^x, \hat{s}_j^y, \hat{s}_j^z)$  and  $\hat{S}_j = (\hat{S}_j^x, \hat{S}_j^y, \hat{S}_j^z)$  are the spin operators for the conduction electron and the spin-1 local spin at the  $j$  site, respectively.  $J > 0$  is the antiferromagnetic Kondo exchange coupling, and the nearest-neighbor hopping  $t$  is set to unity as a unit of energy. To represent the strong Ising anisotropy, we set  $D = 1$  for simplicity in this paper. Without loss of generality, we can assume that the transverse field  $h$  is along the  $x$ -direction.

In the presence of  $h$ , the  $z$ -component of the total spins is not conserved. It is important to choose the bases with which the Hamiltonian in Eq. (1) is block-diagonalized. For this, we need to find the operators that commute with the Hamiltonian in Eq. (1). The total number operator  $\hat{N}_c = \sum_{i,\sigma} \hat{c}_{i\sigma}^\dagger \hat{c}_{i\sigma}$  and the total spin inversion operator  $\hat{P} = \prod_{j=1}^N \hat{P}_j$  meet this requirement. The local spin inversion operator  $\hat{P}_j$  acts on the local bases for the conduction electrons as follows:

$$\begin{aligned} \hat{P}_j |\text{vac}\rangle_j &= |\text{vac}\rangle_j, \quad \hat{P}_j |\uparrow\rangle_j = |\downarrow\rangle_j, \\ \hat{P}_j |\downarrow\rangle_j &= |\uparrow\rangle_j, \quad \hat{P}_j |\uparrow\downarrow\rangle_j = |\downarrow\uparrow\rangle_j, \end{aligned} \quad (2)$$

where  $|\text{vac}\rangle_j$  indicates the empty state for the  $j$  site,  $|\sigma\rangle_j = \hat{c}_{j\sigma}^\dagger |\text{vac}\rangle_j$ , and  $|\uparrow\downarrow\rangle_j = \hat{c}_{j\uparrow}^\dagger \hat{c}_{j\downarrow}^\dagger |\text{vac}\rangle_j$ . For the local spins,

$$\hat{P}_j |\uparrow\uparrow\rangle_j = |\downarrow\downarrow\rangle_j, \quad \hat{P}_j |0\rangle_j = |0\rangle_j, \quad \hat{P}_j |\downarrow\downarrow\rangle_j = |\uparrow\uparrow\rangle_j, \quad (3)$$

where the local bases for the local spins are the eigenstates for  $\hat{S}_j^z$ :  $|\uparrow\uparrow\rangle_j$ ,  $|0\rangle_j$ , and  $|\downarrow\downarrow\rangle_j$  with the eigenvalues 1, 0, and  $-1$ , respectively. The eigenvalues of  $\hat{P}_j$  are  $P_j = \pm 1$  since  $\hat{P}_j^2 = 1$ .

The eigenstates of  $\hat{P}_j$  for the conduction electrons are sum-

marized as

$$\begin{aligned} |\text{vac}\rangle_j \cdots P_j &= 1, \\ \hat{c}_{j,e}^\dagger |\text{vac}\rangle_j &:= \frac{1}{\sqrt{2}}(|\uparrow\rangle_j + |\downarrow\rangle_j) \cdots P_j = 1, \\ \hat{c}_{j,o}^\dagger |\text{vac}\rangle_j &:= \frac{1}{\sqrt{2}}(|\uparrow\rangle_j - |\downarrow\rangle_j) \cdots P_j = -1, \\ \hat{c}_{j,o}^\dagger \hat{c}_{j,e}^\dagger |\text{vac}\rangle_j &:= |\uparrow\downarrow\rangle_j \cdots P_j = -1. \end{aligned} \quad (4)$$

Here,  $\hat{c}_{j,e(o)}^\dagger$  is the creation operator for the conduction electron with even (odd) parity. They are defined as

$$\hat{c}_{j,e}^\dagger = \frac{1}{\sqrt{2}}(\hat{c}_{j\uparrow}^\dagger + \hat{c}_{j\downarrow}^\dagger), \quad \hat{c}_{j,o}^\dagger = \frac{1}{\sqrt{2}}(\hat{c}_{j\uparrow}^\dagger - \hat{c}_{j\downarrow}^\dagger). \quad (5)$$

The eigenstates of  $\hat{P}_j$  for the local spins are given as

$$\begin{aligned} |\text{EV}\rangle_j &:= \frac{1}{\sqrt{2}}(|\uparrow\uparrow\rangle_j + |\downarrow\downarrow\rangle_j) \cdots P_j = 1, \\ |0\rangle_j \cdots P_j &= 1, \\ |\text{OD}\rangle_j &:= \frac{1}{\sqrt{2}}(|\uparrow\uparrow\rangle_j - |\downarrow\downarrow\rangle_j) \cdots P_j = -1. \end{aligned} \quad (6)$$

With these bases, the Hamiltonian in Eq. (1) is rewritten as

$$\begin{aligned} \hat{H} &= -t \sum_{j=1}^{N-1} \sum_{p=e,o} \left( \hat{c}_{j,p}^\dagger \hat{c}_{j+1,p} + \hat{c}_{j+1,p}^\dagger \hat{c}_{j,p} \right) \\ &\quad + J \sum_{j=1}^N \left( \hat{s}_j^x \hat{S}_j^x + \hat{s}_j^y \hat{S}_j^y + \hat{s}_j^z \hat{S}_j^z \right) - h \sum_{j=1}^N \left( \hat{s}_j^x + \hat{S}_j^x \right) \\ &\quad - D \sum_{j=1}^N \left( 1 - |0\rangle_j \langle 0|_j \right), \end{aligned} \quad (7)$$

and the spin operators are represented in the new bases as

$$\hat{s}_j^x = \frac{1}{2} \left( \hat{c}_{j,e}^\dagger \hat{c}_{j,e} - \hat{c}_{j,o}^\dagger \hat{c}_{j,o} \right), \quad (8)$$

$$\hat{s}_j^y = \frac{i}{2} \left( \hat{c}_{j,e}^\dagger \hat{c}_{j,o} - \hat{c}_{j,o}^\dagger \hat{c}_{j,e} \right), \quad (9)$$

$$\hat{s}_j^z = \frac{1}{2} \left( \hat{c}_{j,e}^\dagger \hat{c}_{j,o} + \hat{c}_{j,o}^\dagger \hat{c}_{j,e} \right), \quad (10)$$

$$\hat{S}_j^x = |\text{EV}\rangle_j \langle 0|_j + |0\rangle_j \langle \text{EV}|_j, \quad (11)$$

$$\hat{S}_j^y = i \left( |0\rangle_j \langle \text{OD}|_j - |\text{OD}\rangle_j \langle 0|_j \right), \quad (12)$$

$$\hat{S}_j^z = |\text{EV}\rangle_j \langle \text{OD}|_j + |\text{OD}\rangle_j \langle \text{EV}|_j. \quad (13)$$

The DMRG calculations have been carried out in these bases in each of the subspaces specified by the electron number  $N_c$  and the total spin parity  $P = \pm 1$  (the eigenvalue of  $\hat{P}$ ).

Before closing this section, let us comment on the particle-hole symmetry. The Hamiltonian in Eq. (7) is invariant under the particle-hole transformation

$$\hat{c}_{j,e} \rightarrow (-1)^j \hat{c}_{j,o}^\dagger, \quad \hat{c}_{j,o} \rightarrow (-1)^{j+1} \hat{c}_{j,e}^\dagger. \quad (14)$$

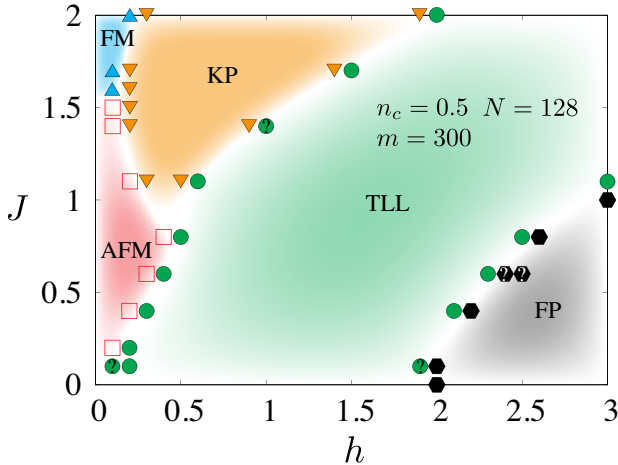


**Fig. 1.** (Color online) Ground-state  $h$ - $J$  phase diagram for  $N = 128$  and  $n_c = 0.5$ . Each phase is identified by the long-distance behavior of the spin-spin correlation functions  $\chi_z^{sc}(r)$  and  $\chi_z^S(r)$ . They do not decay and are finite in the Ising-ordered phases, while they decay exponentially in the KP and FP phases. In the TLL phase, they show a power-law decay. Symbols with “?” near phase boundaries indicate that the ground state is not identified within the system sizes  $N \leq 128$  and the cutoff  $m = 300$ .

The filling of the conduction electrons  $n_c$  changes under the transformation as follows:

$$n_c = \frac{N_c}{N} = \frac{1}{N} \sum_{j=1}^N \sum_{p=e,o} \langle \hat{c}_{j,p}^\dagger \hat{c}_{j,p} \rangle \rightarrow 2 - n_c, \quad (15)$$

where  $\langle \hat{A} \rangle$  represents the ground-state expectation value of the operator  $\hat{A}$ . Considering Eq. (15), one can easily find that systems with the filling  $n_c$  are equivalent to those for  $2 - n_c$  and it is sufficient to consider  $n_c \leq 1$ .

Since the parity index for the conduction electrons changes through Eq. (14), the total spin parity for the electrons depends on the electron number  $N_c$ . It is invariant for  $N_c$  being even, while it changes for odd  $N_c$ . Since the particle-hole transformation does not affect the parity for the local spins, the total spin parity is invariant if  $N_c$  is even, while it changes if  $N_c$  is odd. Thus, systems for  $n_c > 1$  can be trivially mapped to those for  $n_c < 1$  and it is sufficient to consider  $n_c \leq 1$ .

### 3. Results

In this section, we will show the numerical results in detail. DMRG calculations have been carried out for  $N = 32, 64, 96, 128$  and with at least  $m = 200$  states kept in the truncation procedures. We will mainly discuss the results for  $N = 128$ . If necessary, the  $N$  and  $m$  dependences are discussed. In the following, we will first show the  $h$ - $J$  phase diagram for  $n_c = 0.5$  and then discuss the physical quantities such as the magnetizations, the correlation functions, and the critical properties. For other values of  $n_c$ , the results are discussed in Sect. 3.5, in which qualitatively similar phase diagrams are obtained with some new phases.

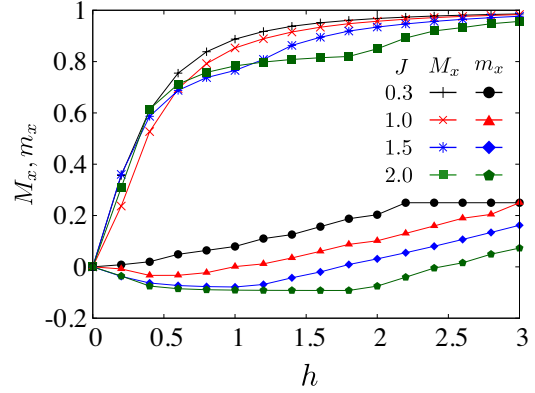


**Fig. 2.** (Color online)  $h$  dependences of  $M_x$  and  $m_x$  for  $J = 0.3, 1.0, 1.5$ , and  $2.0$ , and  $N = 128$ ,  $n_c = 0.5$  with the cutoff  $m = 200$ .  $M_x$  represents the local spins and  $m_x$  represents the conduction electrons. See Eq. (18).

#### 3.1 Phase diagram

Let us first show the ground-state  $h$ - $J$  phase diagram determined by the DMRG method for the typical conduction electron filling  $n_c = 0.5$ . Here, we will explain the overall features and properties of phases appearing in the diagram and will discuss various physical quantities later in this section.

Figure 1 shows the  $h$ - $J$  phase diagram for  $n_c = 0.5$ . There are various phases such as FM, antiferromagnetic (AFM), the Tomonaga-Luttinger liquid (TLL), Kondo plateau (KP) (we will explain the meaning later), and fully polarized (FP) phases. Each of the phases shows a characteristic long-distance asymptotic dependence in the spin-spin correlation functions such as

$$\chi_z^S(r) := \langle \hat{S}_{r+N/2}^z \hat{S}_{N/2}^z \rangle, \quad \chi_z^{sc}(r) := \langle \hat{s}_{r+N/2}^z \hat{s}_{N/2}^z \rangle. \quad (16)$$

The FM and AFM orders are Ising-like, which are possible even in one-dimensional systems at zero temperature. These phases appear for small  $h$ . In particular, the FM phase emerges for large  $J$  and small  $n_c$  (see also Sect. 3.5). The spin-spin correlation functions do not vanish as  $r \rightarrow \infty$  in these phases, which is the signature of symmetry breaking.

In the KP phase, tightly bound local Kondo “doublets” are formed by the conduction electrons and the local spins, and one of the two components gains the magnetic energy due to  $h$ . Note that the magnitudes of the local spin and the conduction electron spins are different in our model. Destroying such a tightly bound doublet requires a large magnetic field  $\sim J$ . This is reflected in the pseudoplateau in the magnetization (Fig. 2) and in the local spin-spin correlation (Fig. 3):

$$\langle \hat{s} \cdot \hat{S} \rangle := \frac{1}{N} \sum_{j=1}^N \langle \hat{s}_j \cdot \hat{S}_j \rangle. \quad (17)$$

We call this phase the “Kondo plateau” after these observations. As will be discussed in Sect. 3.3, the spin-spin correlation functions [Eq. (16)] decay exponentially for  $r \rightarrow \infty$ , which indicates that the spin excitations have a finite gap.

In a wide range of the parameter space, the TLL phase appears, where the spin-spin correlation functions exhibit

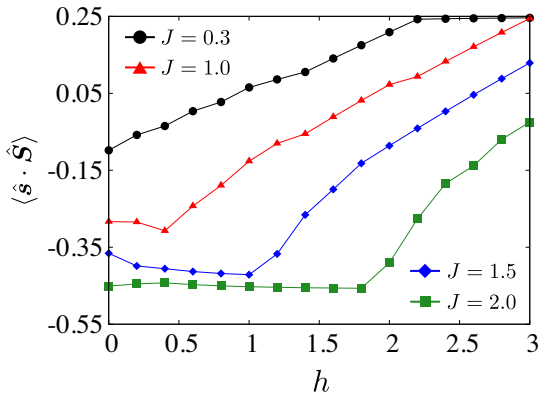


**Fig. 3.** (Color online)  $h$  dependence of  $\langle \hat{s} \cdot \hat{S} \rangle$ , the correlation between the local spins and the electron spins, for  $J = 0.3, 1.0, 1.5$ , and  $2.0$ , and  $N = 128$ ,  $n_c = 0.5$  with the cutoff  $m = 200$ .

power-law decay, which indicates quasi-long-range order. Strictly speaking, it is “TLL” for the charge sector in other phases, but here, we use the name TLL in order to distinguish this phase and others by focusing on the spin sector only. For sufficiently high fields, the FP state appears and this phase is a trivial one expected in the band-shift picture due to the external magnetic field  $h$ .

### 3.2 Magnetization curve and Kondo correlations

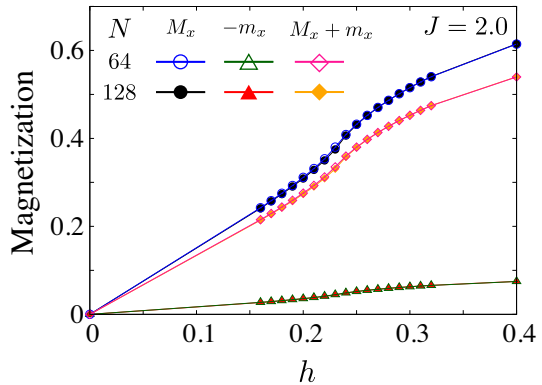
Now, we discuss the response of the ground state against the external transverse magnetic field  $h$ . One of the most relevant quantities for experimental studies is the magnetization, and let us discuss this.

Figure 2 shows the magnetizations along the  $x$ -direction,

$$M_x = \frac{1}{N} \sum_{j=1}^N \langle \hat{S}_j^x \rangle, \quad m_x = \frac{1}{N} \sum_{j=1}^N \langle \hat{s}_j^x \rangle, \quad (18)$$

as a function of  $h$  for several values of  $J$  for  $n_c = 0.5$ .  $M_x$  is induced as  $h$  increases, and around  $h \sim 3.0$ , the moment reaches the saturated value 1 for all  $J$ . Note that for larger  $J$ ,  $J = 2.0$  and  $J = 1.5$ ,  $M_x$  exhibits nonmonotonic  $h$  dependence. For example, for  $J = 2.0$ , below  $h = h_{\text{KP}} \approx 1.92$ ,  $M_x$  monotonically increases as if the full moment were  $\sim 0.8$  and exhibits (almost) no  $h$  dependence between  $h \sim 1$  and  $h_{\text{KP}}$ . Correspondingly,  $m_x$  decreases for small  $h$  and is almost constant with a negative value. In contrast, for  $J = 0.3$ , it increases monotonically and reaches the saturated value  $1/4$  at  $h \approx 2.2$ . Note that  $m_x$  for large  $J$  also starts to increase at  $h = h_{\text{KP}}$ .

To understand this nonmonotonic  $h$  dependence, we analyze the correlation between the conduction electron spins and the local spins:  $\langle \hat{s} \cdot \hat{S} \rangle$  [Eq. (17)]. Figure 3 shows the  $h$  dependence of  $\langle \hat{s} \cdot \hat{S} \rangle$ . For  $J = 2.0$ ,  $\langle \hat{s} \cdot \hat{S} \rangle \approx -0.45$ , and this means that the electron and the local spin are almost frozen, forming an antiparallel configuration, which can also be seen in Fig. 2. Since the magnitudes of the two are different, a residual moment remains. This residual moment aligns along the external field  $h$ , leading to the positive  $M_x$  and the negative  $m_x$  in Fig. 2, since the residual moment is parallel to the local spin. This indicates that the plateau in  $M_x$  is due to the



**Fig. 4.** (Color online) Magnetizations  $M_x$  and  $m_x$  as functions of  $h$  near the phase boundary between the FM and KP phases for  $J = 2.0$ ,  $N = 64, 128$ , and  $n_c = 0.5$  with the cutoff  $m = 200$ . Note that  $-m_x$  (triangles) is plotted for the conduction electron.

strong Kondo correlations; the “spin molecule” is formed between the conduction electron and the local spin. Above  $h_{\text{KP}}$ , this molecule is resolved and  $M_x$ ,  $m_x$ , and  $\langle \hat{s} \cdot \hat{S} \rangle$  start to increase. The transition at  $h = h_{\text{KP}}$  separates the KP and TLL phases. Unfortunately, it is difficult to judge whether the transition is first- or second-order in the present calculations for  $N = 128$  and  $m = 500$ , although there are some indications that it is the second-order; in the KP phase, the correlation lengths of the spin-spin correlation functions seem to diverge toward the phase boundary at  $h = h_{\text{KP}}$ , but their  $m$  dependence does not saturate.  $M_x$ ,  $m_x$ , and  $\langle \hat{s} \cdot \hat{S} \rangle$  exhibit abrupt changes without discontinuity at  $h = h_{\text{KP}}$  when their  $N$  dependence is analyzed. For the TLL side, the spin-spin correlation functions show power-law decay, which means that the correlation length is infinite.

At low fields, there is another phase transition that separates the KP and Ising-ordered phases for  $J = 2.0$  and 1.5. Figure 4 shows the low-field magnetization curve near the transition. The phase boundary corresponds to the field where  $M_x$  shows a (metamagnetic-like) steep increase as a function of the field;  $h_c \sim 0.24$  for  $J = 2.0$ . Although it is not direct evidence for the phase transition, it suggests that there is some anomaly at  $h = h_c$ . We will discuss this point in Sect. 3.3 by analyzing correlation functions, and the low-field phase turns out to be an Ising FM state for  $J = 2.0$  and 1.5. For smaller  $J = 0.3$ , there is no KP phase and there is one transition from the Ising AFM to TLL phases as  $h$  increases. For  $J = 1.0$ , it seems that there is a small region of the KP phase between the FM and TLL phases around  $h = 0.4$  (see Figs. 2 and 3).

### 3.3 Correlation functions

As discussed above, there are various phases as functions of  $J$  and  $h$ . To clarify the nature of each phase, analyzing the correlation functions, e.g., Eq. (16), is important. One can unveil the spatial modulation and the long-distance asymptotic behavior by examining appropriate correlation functions. In our calculations, the cutoff  $m$  is kept up to 500 and the system size  $N$  to 128. In the following, we will show the  $m$  and  $N$  dependences of the correlation functions in the Ising-ordered

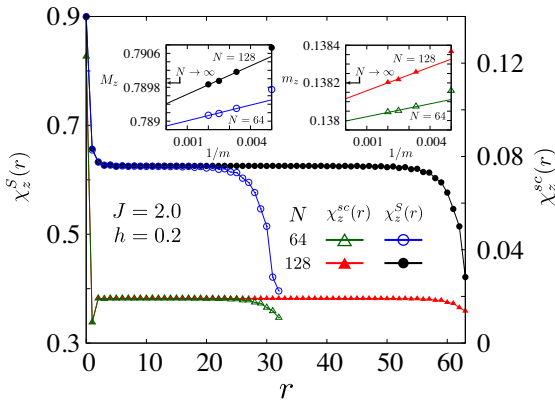


**Fig. 5.** (Color online)  $r$  dependence of the spin-spin correlation functions  $\chi_z^S(r)$  and  $\chi_z^{sc}(r)$  for  $N = 64$  and  $128$  inside the FM phase:  $J = 2.0$ ,  $h = 0.2$ , and  $n_c = 0.5$  with the cutoff  $m = 200$ . The suppression for  $r \sim N/2$  is due to the boundary effects. Inset:  $m$  dependences of the magnetizations  $M_z$  and  $m_z$ . Here,  $M_z^2 = \chi_z^S(N/4)$  and  $m_z^2 = \chi_z^{sc}(N/4)$ . The lines represent the linear fits by using the data for  $m = 300, 400$ , and  $500$ . The arrows indicate the magnetizations extrapolated to  $1/N \rightarrow 0$  by using the extrapolated values  $1/m \rightarrow 0$  for  $N = 64$  and  $128$ , which remain finite.

phases and discuss the finite size effects. In the other phases, they are very small.

The Ising-ordered phases are stabilized for small  $h$ . When  $J$  is large, the FM phase appears and  $\chi_z^S(r)$  and  $\chi_z^{sc}(r)$  [Eq. (16)] exhibit long-range correlations. In the FM phase, the magnetization along the  $z$ -direction is estimated to be  $M_z^2 = \lim_{r \rightarrow \infty} \chi_z^S(r)$  and  $m_z^2 = \lim_{r \rightarrow \infty} \chi_z^{sc}(r)$ . Figure 5 shows the  $r$  dependence of  $\chi_z^S(r)$  and  $\chi_z^{sc}(r)$  for  $J = 2.0$  and  $h = 0.2$ , i.e., in the FM phase. One can see that  $\chi_z^S(r)$  and  $\chi_z^{sc}(r)$  do not decay for a long distance except for the effect of the open boundary, which indicates that the system is in the FM state. The inset of Fig. 5 shows the cutoff  $m$  dependence of the magnetizations  $M_z^2 = \chi_z^S(N/4)$  and  $m_z^2 = \chi_z^{sc}(N/4)$  for  $N = 64$  and  $128$ . Here, we replace  $r \rightarrow \infty$  by  $r = N/4$ . Extrapolating them to  $1/m \rightarrow 0$  and then  $1/N \rightarrow 0$ , we obtain  $M_z \sim 0.79$  and  $m_z \sim 0.14$ . Thus, this analysis confirms that the system is in the FM phase.

Let us now discuss the nature of this FM phase. As shown in Fig. 3,  $\langle \hat{s} \cdot \hat{S} \rangle$  is negative, which means that the local spins and conduction electron spins are antiparallel with each other owing to the strong Kondo exchange coupling  $J$ . This kind of FM phase was also found in the  $S = 1/2$  Kondo lattice model.<sup>33–36</sup> In order for the conduction electrons to gain the kinetic energy, the conduction electrons hop to the neighboring sites with their spins antiparallel to the local ones.<sup>47</sup> Actually, the FM phase is stabilized for small filling, since the conduction electrons can easily traverse. See also Sect. 3.5 for the phase diagrams for  $n_c \neq 0.5$ .

For small  $J$  and  $h$ , the AFM phase appears. Figures 6(a) and 6(b) show the  $r$  dependence of  $\chi_z^S(r)$  and  $\chi_z^{sc}(r)$ , respectively, for  $J = 0.3$  and  $h = 0.2$ .  $\chi_z^S(r)$  shows a four-site-periodicity structure and no decay for large  $r$ . This structure becomes clearer and shows an “up-up-down-down” structure as  $J$  increases as shown in Figs. 6(c) and 6(d) for  $J = 1.0$ . Figure 7 shows the cutoff  $m$  dependence of the AFM moments for

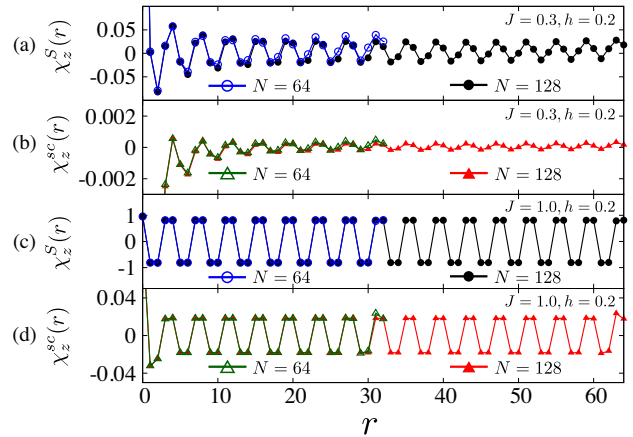


**Fig. 6.** (Color online)  $r$  dependence of the spin-spin correlation functions for  $N = 64$  (open symbols),  $128$  (filled symbols), and  $n_c = 0.5$  with the cutoff  $m = 200$ : (a)  $\chi_z^S(r)$  for  $(J, h) = (0.3, 0.2)$ , (b)  $\chi_z^{sc}(r)$  for  $(J, h) = (0.3, 0.2)$ , (c)  $\chi_z^S(r)$  for  $(J, h) = (1.0, 0.2)$ , and (d)  $\chi_z^{sc}(r)$  for  $(J, h) = (1.0, 0.2)$ . One can see an “up-up-down-down” structure.

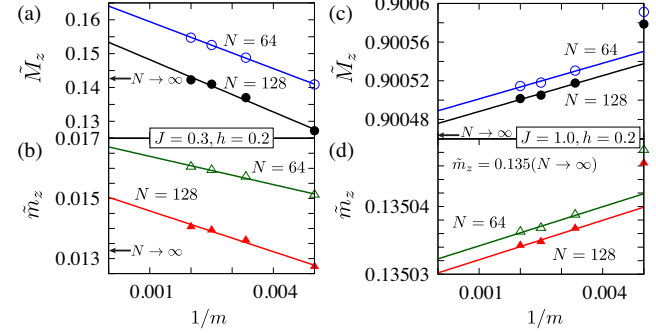


**Fig. 7.** (Color online) Cutoff  $m$  dependence of the AFM moments  $\tilde{M}_z$  and  $\tilde{m}_z$  for  $N = 64$  (open symbols) and  $128$  (filled symbols) inside the AFM phases with  $n_c = 0.5$ : (a)  $\tilde{M}_z$  for  $(J, h) = (0.3, 0.2)$ , (b)  $\tilde{m}_z$  for  $(J, h) = (0.3, 0.2)$ , (c)  $\tilde{M}_z$  for  $(J, h) = (1.0, 0.2)$ , and (d)  $\tilde{m}_z$  for  $(J, h) = (1.0, 0.2)$ . The lines represent the linear fits by using the data for  $m = 200, 300, 400$ , and  $500$  for  $(J, h) = (0.3, 0.2)$  and  $m = 300, 400$ , and  $500$  for  $(J, h) = (1.0, 0.2)$ .

$N = 64$  and  $128$ . Here, the AFM moments  $\tilde{M}_z^2$  and  $\tilde{m}_z^2$  are defined as the average values of  $|\chi_z^{S,sc}(r)|$  from  $r = N/4 - 1$  to  $N/4 + 2$ . The AFM moments in the thermodynamic limit are estimated to be  $(\tilde{M}_z, \tilde{m}_z) \sim (0.14, 0.013)$  for  $(J, h) = (0.3, 0.2)$  and  $(\tilde{M}_z, \tilde{m}_z) \sim (0.9, 0.13)$  for  $(J, h) = (1.0, 0.2)$ .

The main origin of this AFM state is expected to be the RudermanKittelKasuyaYosida (RKKY) interactions.<sup>48–50</sup> When the Kondo interaction  $J$  is small, the  $J$  term can be regarded as a perturbation, and thus the lowest-order interaction between the local spins is the RKKY interaction mediated by conduction electrons. To simplify the discussion, consider the weak-coupling limit. Since  $D = 1 \gg J$ , the large  $D$  prohibits the local spin from flipping by  $\pm 1$  and it leads to the Ising-like interaction between the local spins  $J_{\text{eff}}$  given by

$$J_{\text{eff}}(q) \sim \left( J + \frac{J^2}{2D} \right)^2 \chi_{z0}^{sc}(q). \quad (19)$$

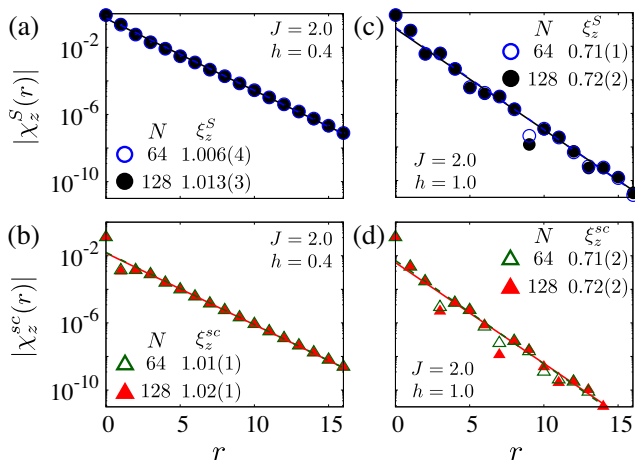


**Fig. 8.** (Color online)  $r$  dependence of the spin-spin correlation functions for  $N = 64$  (open symbols), 128 (filled symbols), and  $n_c = 0.5$  with the cutoff  $m = 200$  in the KP phase: (a)  $|\chi_z^S(r)|$  for  $(J, h) = (2.0, 0.4)$ , (b)  $|\chi_z^{sc}(r)|$  for  $(J, h) = (2.0, 0.4)$ , (c)  $|\chi_z^S(r)|$  for  $(J, h) = (2.0, 1.0)$ , and (d)  $|\chi_z^{sc}(r)|$  for  $(J, h) = (2.0, 1.0)$ . The (dashed) lines represent the fit by  $A \exp(-r/\xi_z^S)$  for  $N = 128$  (64), where  $A$  and  $\xi_z^S$  are the fitting parameters.

Here,  $\chi_{z0}^{sc}(q)$  represents the  $z$  component of the static spin susceptibility with the wavenumber  $q$  for the noninteracting conduction electrons. The dominant Fourier component of Eq. (19) is the one with  $q = 2k_F^0$ , where  $k_F^0$  is the Fermi wavenumber for  $J = h = 0$ . Thus, it is natural to expect that the period of the oscillation in  $\chi_z^S(r)$  corresponds to the inverse of  $2k_F^0$ . Indeed, when  $n_c = 1/2$  and  $h = 0$ , the wavelength is estimated to be  $2\pi/(2k_F^0) \sim 2/n_c = 4$ , which is consistent with the “up-up-down-down” structure shown in Fig. 6. Since  $\chi_z^{sc}(r)$  is related to the interband spin fluctuations under a finite  $h$ , this argument (by setting  $h = 0$ ) is qualitatively valid for  $h > 0$ . As will be discussed in Sect. 3.5,  $\chi_z^{sc}(r)$  has another structure corresponding to  $6k_F^0$  for other fillings.

Now, we discuss the phases with a gap in the spin sector. In general, when a target sector possesses a finite excitation gap, the corresponding correlation function  $\chi(r)$  decays exponentially as  $r \rightarrow \infty$ . The magnitude of the gap is characterized by the correlation length  $\xi$  defined by  $\chi(r) \sim \exp(-r/\xi)$ . In our phase diagram (Fig. 1), there are three types of such gapped states. One is the FP phase, which is a trivial state for high magnetic fields. The second is the KP phase and the third is the Ising-ordered FM and AFM phases as discussed previously.

Let us first discuss the FP phase. When  $h$  is much larger than all the other parameters  $t$ ,  $J$ , and  $D$ , the lower conduction electron band split by  $h$  is filled with  $N_c$  electrons (we are considering the case with  $n_c \leq 1$ ). Flipping a single spin generates interband excitations and requires a finite energy  $\sim h$ . Thus, since  $\chi_z^{sc}(r)$  measures the transverse spin excitations with respect to the direction parallel to  $h$  in the  $x$ -direction,  $\chi_z^{sc}(r)$  should decay exponentially.

For the KP phase, the directions of the local and electron spins are opposite and they form spin molecules due to the large  $J$  as discussed in Sect. 3.2. Thus, flipping either local

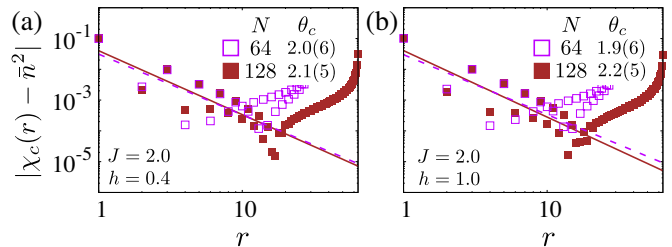


**Fig. 9.** (Color online)  $r$  dependence of the charge correlation function  $|\chi_c(r) - \bar{n}^2|$  for  $N = 64$  (open symbols), 128 (filled symbols),  $n_c = 0.5$  with the cutoff  $m = 200$  in the KP phase: (a)  $(J, h) = (2.0, 0.4)$  and (b)  $(J, h) = (2.0, 1.0)$ .  $\bar{n}^2$  is the average value of  $\chi_c(r)$  from  $r = 20$  to 25 for  $N = 64$  and  $r = 31$  to 40 for  $N = 128$ . The (dashed) lines represent the fit by  $Ar^{-\theta_c}$  for  $N = 128$  (64) in the range  $1 \leq r \leq 10$ .

or conduction electron spins requires a finite energy  $\Delta E \sim J$  corresponding to the bound-state energy for the tightly bound spins. This means that the ground-state wavefunction is well approximated by the direct product state of local ones. For the single-site (i.e.,  $N = 1$ ) model with  $N_e = 1$ , there is a level crossing for  $h \sim J$ ; the Kondo doublet-like state is destabilized for large magnetic fields. This is indeed consistent with our DMRG results and shows a phase transition between the KP and TLL phases for  $h \sim J$ . Figures 8(a) and 8(b) [8(c) and 8(d)] show the  $r$  dependence of  $\chi_z^S(r)$  and  $\chi_z^{sc}(r)$ , respectively, for  $(J, h) = (2.0, 0.4)$  [(2.0, 1.0)] in the KP phase. The linear decay in the semilog plot means that  $\chi_z^S(r)$  and  $\chi_z^{sc}(r)$  decay exponentially. By fitting the data, we obtain the correlation lengths  $\xi_z^S$  and  $\xi_z^{sc}$ ; they are similar and  $\xi_z^S \simeq \xi_z^{sc} \sim 1$  for these parameter sets. This is naturally understood by noting that the correlation lengths are determined by the “strength” of the spin molecules. These short correlation lengths indicate that the KP phase is well described by the direct product of the local wavefunction as discussed above.

Figure 9 shows the  $r$  dependence of the charge correlation function  $\chi_c(r)$ , which is defined as

$$\chi_c(r) := \langle \hat{n}_{r+N/2} \hat{n}_{N/2} \rangle. \quad (20)$$

It decays to a constant value  $\bar{n}^2$  up to  $r \sim 10$ , and for larger  $r$ , the data are masked by the boundary effects. Apart from this boundary effect, it shows power-law behavior as  $\chi_c(r) - \bar{n}^2 \sim 1/r^{\theta_c}$ . Note that  $\bar{n}^2$  is a fitting parameter here and  $\bar{n}^2 \neq n_c^2$ . Thus, in the present numerical calculations, there is no evidence of the charge density wave (CDW) in the KP phase for  $n_c = 0.5$ .

Finally, we discuss the Ising-ordered states, focusing on the universality class of the phase transition between the FM and KP phases. The  $h$  dependences of the correlation length  $\xi_z^S$  and the magnetization  $M_z$  around the phase boundary suggest that the transition belongs to the two-dimensional (2D) Ising universality class. Figure 10 shows the  $h$  dependence of  $M_z$  and  $\xi_z^S$  of  $\chi_z^S(r)$  for  $J = 2.0$ . One can see that

$$M_z \simeq (h_c - h)^{\frac{1}{8}}, \quad \xi_z^S \simeq (h - h_c)^{-1}, \quad \text{with } h_c \sim 0.23 - 0.24. \quad (21)$$

These exponents correspond to  $\beta = 1/8$  and  $\nu = 1$  in the 2D-Ising class, which is consistent with the fact that the system

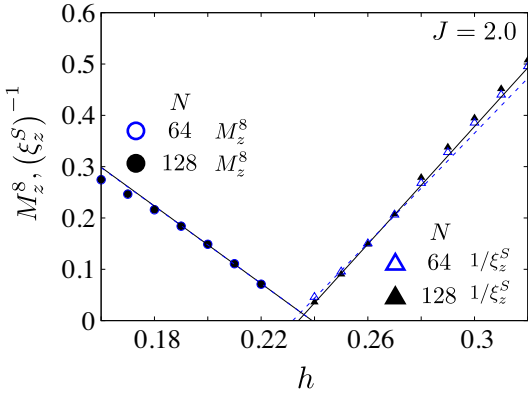


**Fig. 10.** (Color online)  $h$  dependence of  $M_z^8$  and  $1/\xi_z^S$  for  $J = 2.0$  and  $n_c = 0.5$ . Results are obtained from the linear extrapolation to the cutoff  $1/m \rightarrow 0$  by using  $m = 100, 150, 200$ , and  $300$ . The (dashed) lines represent the linear fits for  $M_z^8$  and  $1/\xi_z^S$  for  $N = 128$  ( $64$ ). The fittings are carried out for  $h = 0.19\text{--}0.22$  for  $M_z^8$  and for  $h = 0.24\text{--}0.27$  for  $1/\xi_z^S$ .  $M_z \sim (h_c - h)^{1/8}$  and  $\xi_z^S \sim (h - h_c)^{-1}$  suggest the 2D Ising universality class.

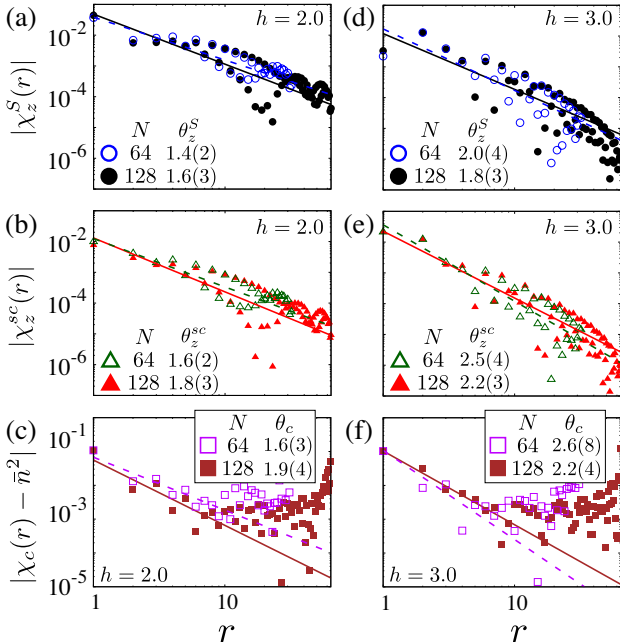


**Fig. 11.** (Color online)  $r$  dependence of the spin-spin and charge correlation functions for  $N = 64$  (open symbols),  $128$  (filled symbols), and  $n_c = 0.5$  with the cutoff  $m = 200$  in the TLL phase: (a)  $|\chi_z^S(r)|$ , (b)  $|\chi_z^{sc}(r)|$ , and (c)  $|\chi_c(r) - \bar{n}|^2$  for  $(J, h) = (2.0, 2.0)$ , and (d)  $|\chi_z^S(r)|$ , (e)  $|\chi_z^{sc}(r)|$ , and (f)  $|\chi_c(r) - \bar{n}|^2$  for  $(J, h) = (2.0, 3.0)$ . The (dashed) lines represent the fit by  $Ar^{-\theta}$  for  $N = 128$  ( $64$ ). The range of the fitting for  $|\chi_c(r) - \bar{n}|^2$  is the same as that in Fig. 9.

possesses the Ising anisotropy. The critical field  $h_c \sim 0.23\text{--}0.24$  is consistent with the metamagnetic field observed in the magnetization in Fig. 4.

Let us close the discussion about correlation functions by examining them in the TLL phase. Figure 11 shows the  $r$  dependence of  $\chi_z^S(r)$ ,  $\chi_z^{sc}(r)$ , and  $\chi_c(r)$  for  $(J, h) = (2.0, 2.0)$  and  $(2.0, 3.0)$ . The results indicate the power-law decay  $\sim 1/r^\theta$ ,

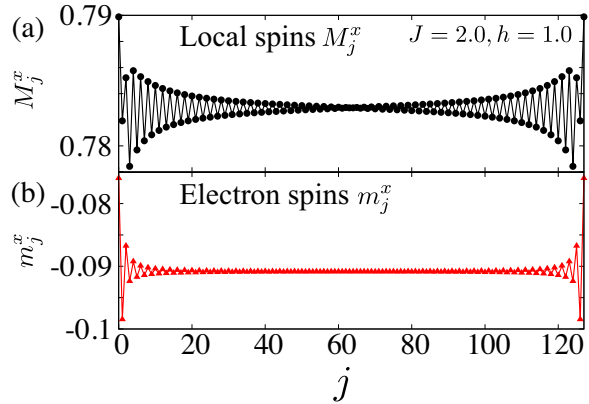


**Fig. 12.** (Color online) Spatial dependence of the magnetizations (a)  $M_j^x$  and (b)  $m_j^x$  for  $N = 128$ ,  $J = 2.0$ ,  $h = 1.0$ , and  $n_c = 0.5$  with the cutoff  $m = 200$  in the KP phase. The oscillations decay exponentially to  $j = 64$  from both the left and right edges. The correlation lengths  $\xi_x^S$  and  $\xi_x^{sc}$  are strongly size-dependent. See the main text.

reflecting the fact that the system is critical, although the numerical accuracy is insufficient for the precise determination of the exponent  $\theta$ . For this, we need more elaborate calculations, which will be tackled as a future problem.

### 3.4 Friedel oscillations

Here, we analyze the spatial dependence of the expectation values:  $M_j^x := \langle \hat{S}_j^x \rangle$  and  $m_j^x := \langle \hat{s}_j^x \rangle$ . Their spatial dependence is affected by the presence of the edges.  $M_j^x$  and  $m_j^x$  show characteristic oscillations and decay<sup>51)</sup>, which reflect the ground state of the system. This is known as Friedel oscillations.<sup>52)</sup>

Figures 12(a) and 12(b) show the spatial dependence of  $M_j^x$  and  $m_j^x$ , respectively, for  $J = 2.0$  and  $h = 1.0$  in the KP phase. The oscillations of these local magnetizations seem to decay exponentially toward the middle of the chain. By fitting the data to the form  $c_1 + c_2 \exp(-j/\xi_x)$  for  $20 < j < 40$ , we can estimate the correlation length  $\xi_x$ . We find that  $\xi_x^S = 10.20$  for  $M_j^x$  and  $\xi_x^{sc} = 8.09$  for  $m_j^x$  for  $N = 64$  and  $\xi_x^S = 19.46$  and  $\xi_x^{sc} = 16.95$  for  $N = 128$  about twice the length of that for  $N = 64$ . This suggests that the system size is much smaller than true  $\xi_x^{S, sc}$ . Because the system is metallic, it is natural to expect that the longitudinal fluctuation is not gapped, i.e.,  $\xi_x^{S, sc} \rightarrow \infty$  in the thermodynamic limit.

When the system is critical, the profile of the oscillation markedly changes. Figures 13(a) and 13(b) show  $M_j^x$  and  $m_j^x$ , respectively, for  $J = 2.0$  and  $h = 3.0$ , where the system is in the TLL phase. The long-range oscillation, which is one of the characteristics of a TLL, is induced by the presence of the edges. The dominant components of this oscillation correspond to two kinds of Fermi wavenumbers  $k_{F\pm}$ , where  $+$  ( $-$ ) indicates the upper (lower) conduction electron band. For  $J = 0$ , they are given as

$$k_{F\pm}^0(h) = \frac{\pi n_c}{2} \mp \arcsin \frac{h}{4 \sin \frac{\pi n_c}{2}}. \quad (22)$$

Suppose the Fermi surface (point) is “small” as expected for the  $S = 1$  Kondo lattice model,<sup>53,54)</sup>  $k_{F\pm}^0$  is identical to  $k_{F\pm}^0$ .

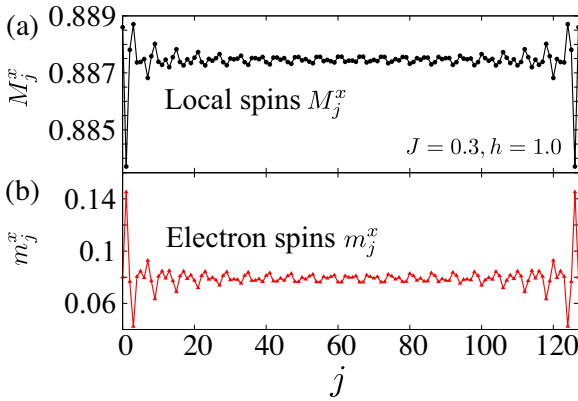


**Fig. 13.** (Color online) Spatial dependence of the magnetizations (a)  $M_j^x$  and (b)  $m_j^x$  for  $N = 128$ ,  $J = 0.3$ ,  $h = 1.0$ , and  $n_c = 0.5$  with the cutoff  $m = 200$  in the TLL phase. The amplitude of the oscillations is so small that it is impossible to judge whether they show exponential or power-law decay.

Absolute values of the Fourier transform  $m_q^x$  of  $m_j^x$  for  $h = 0.6$ , 1.0, and 1.4 with fixed  $J = 0.3$  are shown in Fig. 14. There are two peaks for all the three  $h$ . For example, for  $h = 0.6$ , the two peaks are located at  $q_1 = 1.28$  and  $q_2 = 1.86$ , which are very close to  $2k_{F+}^0(h_{\text{eff}}) = 1.31$  and  $2k_{F-}^0(h_{\text{eff}}) = 1.83$ . Here,  $h_{\text{eff}} = h - JM_x(h = 0.6) = 0.37$  is the effective field for the conduction electrons. Similarly, for  $h = 1.0$  and 1.4, there are two peaks corresponding to  $2k_{F\pm}^0(h_{\text{eff}})$ . This is consistent with the “small Fermi surface”. For larger  $J$ , the analysis based on  $h_{\text{eff}}$  does not work and the spin correlations are not governed by the Fermi points.

### 3.5 Filling dependence

So far, we have discussed the case for  $n_c = 0.5$ . In this subsection, we will briefly show the results for other fillings  $n_c = 0.25, 0.75$ , and 1.0, since most of the phases appearing for  $n_c \neq 0.5$  are similar to those appearing for  $n_c = 0.5$ . One qualitatively different point from the case of  $n_c = 0.5$  is that a CDW state appears in the KP and AFM phases for  $n_c = 0.75$ .

Figures 15(a)–15(c) show the  $h$ - $J$  phase diagrams for  $n_c = 0.25, 0.75$ , and 1.0, respectively. For the smallest filling  $n_c = 0.25$ , the FM phase appears for most of the Ising-ordered phases and the KP and FP phases occupy a wide range of the phase diagram as shown in Fig. 15(a). For the larger fillings, the FM phase disappears and the AFM phase extends to larger  $h$  compared with the smaller fillings. For  $n_c = 0.75$  and 1.0 [Figs. 15(b) and 15(c)], however, there is ambiguity in the long-distance behavior of  $\chi_z^{S,sc}(r)$  for the shaded areas;  $\chi_z^{S,sc}(r)$  for large  $r$  seems to still decay slightly, while the oscillation is similar to that in the AFM phase. We have examined  $\chi_z^{S,sc}(r)$  for the cutoff  $m$  up to 500, but this behavior persists. Thus, the presence of the AFM phase in the shaded areas is considered to be an artifact due to the finite size effects and/or insufficient cutoff number near the phase boundary, although it would be interesting if the reentrant phase diagram as a function of  $h$  was realized. When  $J = 0$  and  $n_c = 0.75$ , the FP phase appears for  $h \gtrsim 3.62$  and for  $n_c = 1.0, h > 4$ .

As mentioned above, the CDW coexists with the AFM and

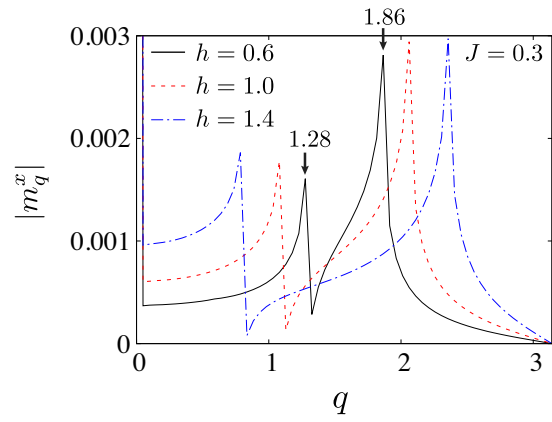


**Fig. 14.** (Color online) Wavenumber  $q$  dependence of  $|m_q^x|$  for  $N = 128$ ,  $J = 0.3$ , and  $n_c = 0.5$  with the cutoff  $m = 200$ . Data for three sets of the magnetic fields ( $h = 0.6, 1.0$ , and 1.4) are shown for clarity and the two peaks in each  $h$  correspond to  $2k_{F\pm}$ . Note that there is a large  $q = 0$  component since  $m_x$  is induced by  $h$ .

KP states for  $n_c = 0.75$  in Fig. 15(b). Figure 16(a) shows the  $r$  dependence of the charge correlation function  $\chi_c(r)$  for  $J = 1.0$  and  $h = 0.2$  in the AFM phase. One can see the oscillation with the wavenumber  $q = \pi/2$ , which corresponds to  $4k_F^0 = \pi/2 \bmod 2\pi$  for  $h = 0$ . This is verified by the direct Fourier transform as shown in Fig. 16(b). A similar CDW with  $q = 4k_F^0$  appears also for  $n_c = 0.8$  and 0.85 (not shown). Figures 16(c) and 16(d) show the cutoff  $m$  and the system size  $N$  dependence of the dominant Fourier component for  $q = \pi/2$ . Extrapolating them to  $1/m \rightarrow 0$  for each  $N$  and then to  $1/N \rightarrow 0$ , we obtain a finite value  $\chi_c(q = \pi/2) \sim 0.022$ . In contrast to  $\chi_c$ , the spin correlations  $\chi_z^S$  and  $\chi_z^{sc}$  are governed by the  $2k_F$  fluctuations as discussed before. The inset of Fig. 16(a) shows  $\chi_z^S(r)$  and there are complex modulations. The main Fourier mode is that for  $q = 3\pi/4$  as shown in Fig. 16(b), which is the  $2k_F^0$  mode. There is another peak for  $q = \pi/4$ , which corresponds to  $6k_F^0 = \pi/4 \bmod 2\pi$ . This is considered to be the coupling mode of the CDW with  $q = 4k_F^0$  and the AFM state with  $q = 2k_F^0$ . In the one-dimensional spin-1/2 Kondo lattice model, the spin density oscillations induced by the presence of a boundary have a two-peak structure corresponding to the  $2k_F^0$  mode and the coupling mode between the spin- and charge-density oscillations.<sup>51)</sup> The amplitude of the latter decreases with increasing system size. Thus, also in our calculations, there is a possibility that the structure corresponding to  $6k_F^0$  disappears in the thermodynamic limit. In two- and infinite-dimensional spin-1/2 Kondo lattice models, CDWs are reported at finite temperatures for  $n_c \simeq 0.5$ .<sup>55,56)</sup> In our DMRG study, however, there is no evidence for the CDW for  $n_c = 0.5$ . More detailed and sophisticated investigations<sup>57,58)</sup> are needed to gain a deep understanding about the emergence of such CDW states, since the amplitudes for the CDW obtained are relatively small.

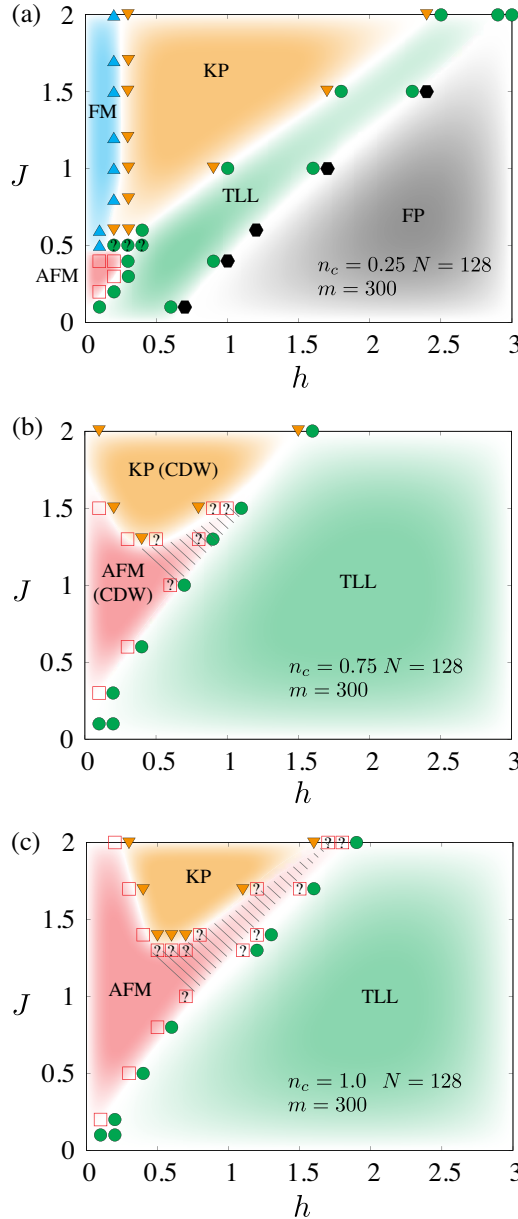


**Fig. 15.** (Color online) Ground-state  $h$ - $J$  phase diagram for (a)  $n_c = 0.25$ , (b)  $n_c = 0.75$ , and (c)  $n_c = 1.0$ . The phases are determined by analyzing the behavior of the correlation functions for  $N = 64$  and  $128$  with the cutoff  $m = 300$ . The symbols represent points where numerical calculations have been carried out, and their type and color distinguish the ground state. For clarity, only the symbols near phase boundaries are indicated. Symbols with “?” near phase boundaries and the shaded area indicate that the ground state is not identified owing to the finite size effects and/or insufficient cutoff  $m$ . See the explanation in the main text. For (b) and (c), the FP phase is located at  $h > 3$ .

#### 4. Discussion and Summary

##### 4.1 Comparison with the experimental results for URhGe

In this section, we compare our results with the experimental results for URhGe. We have studied the simplified one-dimensional model [Eq. (1)], keeping the FM superconductor URhGe in mind. In URhGe, as the external magnetic field  $H$  is applied to the hard axis (b-axis), the SC disappears at

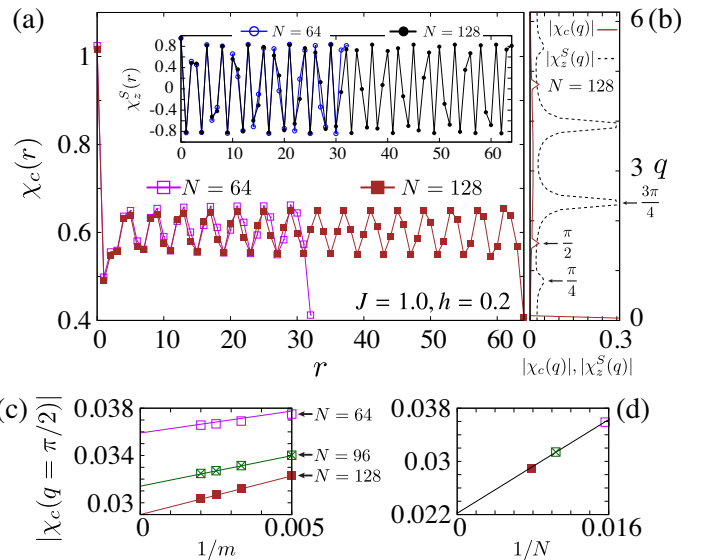


**Fig. 16.** (Color online) Comparison between the charge and spin correlations in the AFM phase for  $n_c = 0.75$ ,  $J = 1.0$ , and  $h = 0.2$  with the cutoff  $m = 400$ . (a) Spatial dependence of  $\chi_c(r)$ . Inset:  $\chi_z^S(r)$  as a function of  $r$ . (b) Fourier transforms  $\chi_c(q)$  and  $\chi_z^S(q)$  for  $\chi_c(r)$  and  $\chi_z^S(r)$ , respectively, for  $N = 128$ . (c) Cutoff  $m$  dependence of  $\chi_c(q = \pi/2)$ . The lines represent the linear fits by using the data for  $m = 200, 300, 400$ , and  $500$ . (d)  $N$  dependence of  $\chi_c(q = \pi/2)$ . The symbols correspond to  $1/m \rightarrow 0$  values for each  $N$  in (c). The line represents the linear fit by using the data for  $N = 64, 96$ , and  $128$ .

$H \sim 2$  T, but it reappears for  $H = 9 \sim 13$  T. In particular, the transition temperature  $T_{\text{sc}}$  is highly enhanced and has a maximum value of 0.42 K for  $H = H_R \sim 12$  T. This enhancement in  $T_{\text{sc}}$  is closely related to the spin reorientation at  $H_R$  and also to the metamagnetism<sup>16)</sup> originating from the tricriticality.<sup>14, 15)</sup>

In our model, metamagnetic enhancement of  $M_x$  appears around  $h_c$  as shown in Fig. 4. This is in sharp contrast to the spin-wave analysis in Ref. 18, where the longitudinal magnetization is essentially given by that for the mean-field approximation. In the DMRG analysis, quantum fluctuations are fully taken into account, which is necessary for the metamagnetic behavior shown in Fig. 4. In the experimental situation, the tricritical point is located at  $T \sim 2\text{--}4$  K<sup>14, 15)</sup>  $> T_{\text{sc}}$ . Thus, the SC dome should be across the first-order line. One might wonder why the SC is induced by the first-order transition since the fluctuations are usually small. However, the NMR experiment<sup>9, 10)</sup> has revealed that there is strong fluctuation even in such a situation owing to the proximity to the tricritical point. As analyzed in detail in Sect. 3.3, the phase transition between the Ising FM and KP phases is second-order with the 2D Ising class. Thus, there is no tricritical point in our model. Nevertheless, it will be interesting to examine whether SC fluctuations are enhanced and also which channels of SC are favored near the phase boundary in future studies. Note that the TLL phase is always next to the FP phase on the low-field side, and also the high-field boundary of the FM phase faces the KP phase, which represents strong Kondo correlations, for the parameter sets we have examined. Thus, various phases com-

pete near the FM phase under transverse fields in the present Kondo lattice model. Generally, in such a situation, there are various fluctuations and it is interesting to examine the possibility of enhanced superconducting fluctuations. We expect that such a situation can capture the physics of URhGe under transverse fields.

#### 4.2 Summary

We have analyzed the  $S = 1$  one-dimensional Kondo lattice model with a uniaxial anisotropy under a transverse field  $h$  by using the DMRG, which is a simplified model for the U-based FM superconductor URhGe and related compounds. We have constructed the ground-state phase diagram as functions of the magnetic field  $h$  and the Kondo exchange coupling  $J$  for several conduction electron fillings. The phase diagram includes various phases such as the Ising-ordered FM and AFM phases, the TLL phase, and the fully polarized (FP) phase. In addition, a (spin) gapped phase appears in moderate  $h$  between the FM and TLL states, where the local and conduction electron spins are tightly bound antiferromagnetically and the magnetization there shows a plateau-like  $h$  dependence. We have dubbed this the Kondo plateau (KP) phase. We have also discussed the metamagnetic behavior when the FM state is destabilized by applying the transverse field  $h$  and found a steep increase in the magnetization near the critical field for the FM phase. This behavior is consistent with the magnetization data for URhGe. Examining the superconducting fluctuation near the critical field is an interesting future direction and is now in progress.

#### Acknowledgment

This work was supported by a Grant-in-Aid for Scientific Research (Grant Nos. 16H01079 and 18K03522) from the Japan Society for the Promotion of Science.

- 
- 1) S. S. Saxena, P. Agarwal, K. Ahilan, F. M. Grosche, R. K. W. Haselwimmer, M. J. Steiner, E. Pugh, I. R. Walker, S. R. Julian, P. Monthoux, G. G. Lonzarich, A. Huxley, I. Sheikin, D. Braithwaite, and J. Flouquet, *Nature* **406**, 587 (2000).
  - 2) D. Aoki, A. Huxley, E. Ressouche, D. Braithwaite, J. Flouquet, J. P. Brison, E. Lhotel, and C. Paulsen, *Nature* **413**, 613 (2001).
  - 3) T. Akazawa, H. Hidaka, T. Fujiwara, T. C. Kobayashi, E. Yamamoto, Y. Haga, R. Settai, and Y. Ōnuki, *J. Phys.: Condens. Matter* **16**, L29 (2004).
  - 4) N. T. Huy, A. Gasparini, D. E. de Nijs, Y. Huang, J. C. P. Klaasse, T. Gortenmulder, A. de Visser, A. Hamann, T. Görlach, and H. v. Löhneysen, *Phys. Rev. Lett.* **99**, 067006 (2007).
  - 5) F. Lévy, I. Sheikin, B. Grenier, and A. D. Huxley, *Science* **309**, 1343 (2005).
  - 6) A. Miyake, D. Aoki, and J. Flouquet, *J. Phys. Soc. Jpn.* **77**, 094709 (2008).
  - 7) E. Hassinger, D. Aoki, G. Knebel, and J. Flouquet, *J. Phys. Soc. Jpn.* **77**, 073703 (2008).
  - 8) D. Aoki, T. D. Matsuda, V. Taufour, E. Hassinger, G. Knebel, and J. Flouquet, *J. Phys. Soc. Jpn.* **78**, 113709 (2009).
  - 9) Y. Tokunaga, D. Aoki, H. Mayaffre, S. Krämer, M.-H. Julien, C. Berthier, M. Horvatić, H. Sakai, S. Kambe, and S. Araki, *Phys. Rev. Lett.* **114**, 216401 (2015).
  - 10) Y. Tokunaga, D. Aoki, H. Mayaffre, S. Krämer, M.-H. Julien, C. Berthier, M. Horvatić, H. Sakai, T. Hattori, S. Kambe, and S. Araki, *Phys. Rev. B* **93**, 201112 (2016).
  - 11) T. Hattori, Y. Ihara, Y. Nakai, K. Ishida, Y. Tada, S. Fujimoto, N. Kawakami, E. Osaki, K. Deguchi, N. K. Sato, and I. Satoh, *Phys. Rev. Lett.* **108**, 066403 (2012).
  - 12) T. Hattori, K. Karube, K. Ishida, K. Deguchi, N. K. Sato, and T. Yamamura, *J. Phys. Soc. Jpn.* **83**, 073708 (2014).
  - 13) S. Sachdev, *Quantum Phase Transitions* (Cambridge University Press, Cambridge, MA, 1999) p. 39.
  - 14) A. Gourgout, A. Pourret, G. Knebel, D. Aoki, G. Seyfarth, and J. Flouquet, *Phys. Rev. Lett.* **117**, 046401 (2016).
  - 15) H. Kotegawa, K. Fukumoto, T. Toyama, H. Tou, H. Harima, A. Harada, Y. Kitaoka, Y. Haga, E. Yamamoto, Y. Ōnuki, K. M. Itoh, and E. E. Haller, *J. Phys. Soc. Jpn.* **84**, 054710 (2015).
  - 16) F. Hardy, D. Aoki, C. Meingast, P. Schweiss, P. Burger, H. v. Löhneysen, and J. Flouquet, *Phys. Rev.* **83**, 195107 (2011).
  - 17) V. P. Mineev, *Phys. Rev. B* **83**, 064515 (2011).
  - 18) K. Hattori and H. Tsunetsugu, *Phys. Rev. B* **87**, 064501 (2013).
  - 19) C. Lörscher, J. Zhang, Q. Gu, and R. A. Klemm, *Phys. Rev. B* **88**, 024504 (2013).
  - 20) V. P. Mineev, *Phys. Rev. B* **90**, 064506 (2014).
  - 21) V. P. Mineev, *Phys. Rev. B* **91**, 014506 (2015).
  - 22) V. P. Mineev, *Phys. Rev. B* **96**, 104501 (2017).
  - 23) Y. Tada, S. Takayoshi, and S. Fujimoto, *Phys. Rev. B* **93**, 174512 (2016).
  - 24) Y. Sherkunov, A. V. Chubukov, and J. J. Betouras, *Phys. Rev. Lett.* **121**, 097001 (2018).
  - 25) T. Nomoto and H. Ikeda, *J. Phys. Soc. Jpn.* **86**, 023703 (2017).
  - 26) A. Daido, T. Yoshida, and Y. Yanase, arXiv:1803.07786.
  - 27) H. Tsunetsugu, M. Sigrist, and K. Ueda, *Rev. Mod. Phys.* **69**, 809 (1997).
  - 28) K. Ueda, T. Nishino, and H. Tsunetsugu, *Phys. Rev. B* **50**, 612 (1994).
  - 29) N. Shibata and K. Ueda, *J. Phys.: Condens. Matter* **11**, 4289 (1999).
  - 30) F. F. Assaad, *Phys. Rev. Lett.* **83**, 796 (1999).
  - 31) J. Otsuki, H. Kusunose, and Y. Kuramoto, *Phys. Rev. Lett.* **102**, 017202 (2009).
  - 32) S. Smerat, U. Schollwöck, I. P. McCulloch, and H. Schoeller, *Phys. Rev. B* **79**, 235107 (2009).
  - 33) M. Troyer and D. Würtz, *Phys. Rev. B* **47**, 2886 (1993).
  - 34) H. Tsunetsugu, M. Sigrist, and K. Ueda, *Phys. Rev. B* **47**, 8345 (1993).
  - 35) G. Honner and M. Gulács, *Phys. Rev. Lett.* **78**, 2180 (1997).
  - 36) G. Honner and M. Gulács, *Phys. Rev. B* **58**, 2662 (1998).
  - 37) I. P. McCulloch, A. Juozapavicius, A. Rosengren, and M. Gulács, *Philos. Mag. Lett.* **81**, 869 (2001).
  - 38) I. P. McCulloch, A. Juozapavicius, A. Rosengren, and M. Gulács, *Phys. Rev. B* **65**, 052410 (2002).
  - 39) A. Juozapavicius, I. P. McCulloch, M. Gulács, and A. Rosengren, *Philos. Mag. B* **82**, 1211 (2002).
  - 40) D. J. Garcia, K. Hallberg, B. Alascio, and M. Avignon, *Phys. Rev. Lett.* **93**, 177204 (2004).
  - 41) S. A. Basylko, P. H. Lundow, and A. Rosengren, *Phys. Rev. B* **77**, 073103 (2008).
  - 42) R. Peters and N. Kawakami, *Phys. Rev. B* **86**, 165107 (2012).
  - 43) C. Thomas, A. S. da Rosa Simões, J. R. Iglesias, C. Lacroix, N. B. Perkins, and B. Coqblin, *Phys. Rev. B* **83**, 014415 (2011).
  - 44) C. Thomas, A. S. da Rosa Simões, C. Lacroix, J. R. Iglesias, and B. Coqblin, *J. Magn. Magn. Mater.* **372**, 247 (2014).
  - 45) M. Koga, G. Zaránd, and D. L. Cox, *Phys. Rev. Lett.* **83**, 2421 (1999).
  - 46) S. R. White, *Phys. Rev. Lett.* **69**, 2863 (1992); *Phys. Rev. B* **48**, 10345 (1993).
  - 47) E. Dagotto, T. Hotta, and A. Moreo, *Phys. Rep.* **344**, 1 (2001).
  - 48) M. A. Ruderman and C. Kittel, *Phys. Rev.* **96**, 99 (1954).
  - 49) T. Kasuya, *Prog. Theor. Phys.* **16**, 45 (1956).
  - 50) K. Yosida, *Phys. Rev.* **106**, 893 (1957).
  - 51) N. Shibata, K. Ueda, T. Nishino, and C. Ishii, *Phys. Rev. B* **54**, 13495 (1996).
  - 52) J. Friedel, *Philos. Mag.* **43**, 153 (1952).
  - 53) M. Yamanaka, M. Oshikawa, and I. Affleck, *Phys. Rev. Lett.* **79**, 1110 (1997).

- 54) M. Oshikawa, Phys. Rev. Lett. **84**, 3370 (2000).  
55) T. Misawa, J. Yoshitake, and Y. Motome, Phys. Rev. Lett. **110**, 246401  
(2013).  
56) J. Otsuki, H. Kusunose, and Y. Kuramoto, J. Phys. Soc. Jpn. **78**, 014702  
(2009); J. Phys. Soc. Jpn. **78**, 034719 (2009).  
57) N. Shibata and C. Hotta, Phys. Rev. B **84**, 115116 (2011).  
58) H. Katsura, J. Phys. A **45**, 115003 (2012).